Safety-Critical Control For a Tilt-Rotor Bicopter Using Control Barrier Function

1st Sepehr Mahfar
Aerospace Engineering Department
Sharif University of Technology
Tehran, Iran
sepehr.mahfar81@gmail.com

2nd Alireza Sharifi
Aerospace Engineering Department
Sharif University of Technology
Tehran, Iran
ar.sharifi@sharif.edu

***Abstract*—This paper presents a safety-critical control strategy For tilt-rotor bicopters utilizing control barrier functions (CBFs). The dynamic model of the bicopter is first established, followed by the design of a linear quadratic regulator (LQR) to achieve trajectory tracking. To formulate a control barrier function, it is crucial for the control input in the altitude-channel to explicitly appear in the equations governing this channel. A command producer is utilized to represent the altitude-channel control input within the dynamic equations. Subsequently, a high-order control barrier function (HOCBF) is designed to maintain safe altitude levels while ensuring trajectory tracking. The approach is validated through simulation, demonstrating the bicopter's ability to avoid unsafe altitude regions while fulfilling control objectives.**

***Index Terms*—control barrier function, bicopter, safety, safe region, obstacle avoidance**

I. Introduction

Unmanned aerial vehicles (UAVs) with novel configurations, such as bicopters [1], have attracted increasing attention due to their lightweight design, mechanical simplicity, and energy efficiency. Unlike quadrotors and other multirotor platforms, the bicopter employs only two tilting rotors, which significantly reduces structural complexity. However, this minimal design introduces severe control challenges since the system is inherently underactuated and exhibits strong nonlinearities.

Classical controllers such as proportional–integral–derivative (PID) [2] can control the system under nominal conditions. Several studies have addressed the stabilization of Euler angles. In [3], the stabilization of a physical bicopter was carried out using a PID controller, where the control input was generated based on the output of a Kalman filter. To achieve this, the Euler angles were estimated by processing the measurements obtained from an inertial measurement unit (IMU) through the Kalman filter. Furthermore, [4] investigated the stabilization of the pitch angle of a bicopter by deriving the transfer function of the pitch channel and employing a PID control strategy. In [5], a PID-based attitude control scheme for the bicopter was first designed and validated in a simulation environment and subsequently implemented in real-world experiments. In [6], a cascade loop control architecture was proposed to regulate both altitude and attitude of the bicopter. In this framework, the outer and inner attitude control loops were designed using feedback from angular rates and the Euler angle measurements of the bicopter, respectively. In [7], the transfer functions of the attitude channels for the bicopter were identified in the frequency domain. Based on the extracted model, PID controller was implemented. Some studies have also applied modern control techniques to bicopter regulation. In [8], a linear model predictive controller (LMPC) was designed using a piecewise affine (PWA) modeling approach for the takeoff and landing phases. To this end, the nonlinear dynamics of the bicopter were linearized under the assumption of small angles. Similarly, in [9], the control of position, altitude, and attitude of the bicopter was achieved using a nonlinear control strategy of the ISKAM type, where the nonlinear dynamic model was derived under the small-angle assumption. In [10], the performance of a linear quadratic gaussian (LQG) controller was evaluated for position control of a bicopter in the presence of disturbances caused by suspended payloads. Despite the effectiveness of these control strategies in achieving stabilization and tracking, they often lack formal guarantees for safety, particularly in the altitude channel. Overshoot phenomena can lead to violations of altitude constraints, posing significant risks during operation. Moreover, the desired altitude commands generated by users or higher-level path planning algorithms may themselves be unsafe or inconsistent with the system's operational constraints. Control barrier functions (CBFs) [11] have recently emerged as a powerful framework to enforce forward invariance of safety sets in nonlinear control systems, By incorporating CBF constraints into the control design, the safety of the system can be ensured in real time. In particular, CBFs have been adopted in quadrotor systems [12] for obstacle avoidance by filtering control input online. For relative degree one constraints, standard CBFs are sufficient. However, in many UAV applications, including the altitude dynamics of the bicopter, the safety constraint is of higher relative degree. In such cases, high order control barrier functions (HOCBFs) [13] provide a systematic way to handle safety constraints that depend on higher-order derivatives of the states.

In this work, a HOCBF-based control architecture is developed for the altitude-channel of a bicopter. The altitude

dynamics are first derived from the full nonlinear model using Newton–Euler relations. A candidate safety function is then formulated to represent the minimum allowable altitude, and the HOCBF framework is employed to guarantee forward invariance of the safe set. The proposed safety-critical control architecture is illustrated in Fig. 1.

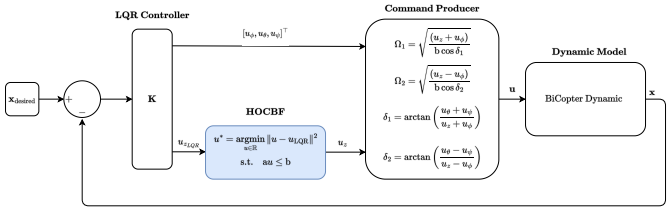

Fig. 1: Block diagram of the proposed safety-critical control architecture

II. Dynamic Modeling of Bicopter

A. Introduction to Coordinate Systems

In this section, the coordinate systems are introduced. The inertial frame is denoted by $\{I\}$ and the body frame is denoted by $\{B\}$ as shown in Fig. 2. The origin of the inertial frame is located at the initial position of the bicopter, and its axes are aligned with the North-East-Down (NED) directions. The body frame is attached to the bicopter, with its origin at the center of mass (CoM) of the vehicle. The x-axis points forward, the y-axis points to the right, and the z-axis points downward.

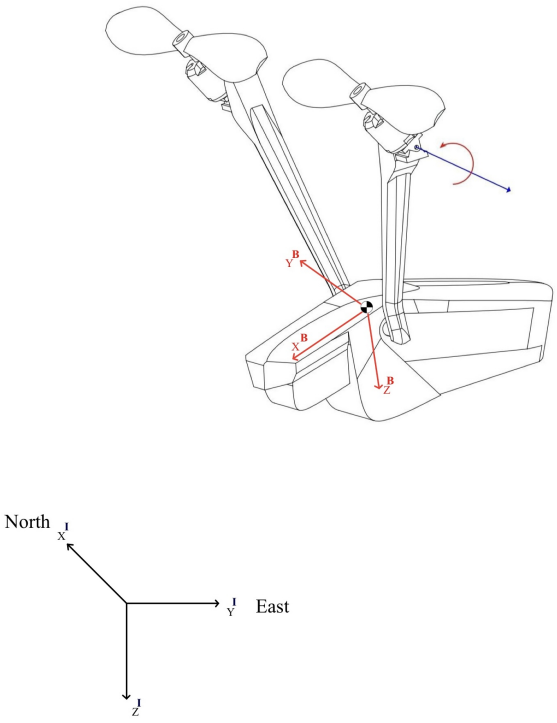

Fig. 2: Inertial and body coordinate systems

B. Forces and Moments

The bicopter is equipped with two rotors that can tilt to provide both lift and control moments. The forces acting on the bicopter in the body frame are given by:

$$[\mathbf{f}]^{\mathrm{B}} = [\mathbf{f}_{\mathrm{g}}]^{\mathrm{B}} + [\mathbf{f}_{\mathrm{d}}]^{\mathrm{B}} + [\mathbf{f}_{\mathrm{t}}]^{\mathrm{B}} \tag{1}$$

where:

$$[\mathbf{f}_{\mathrm{g}}]^{\mathrm{B}} = \begin{bmatrix} -\mathrm{mg}\sin\theta \\ \mathrm{mg}\sin\phi\cos\theta \\ \mathrm{mg}\cos\phi\cos\theta \end{bmatrix} \tag{2}$$

g represents the gravitational acceleration, m is the mass of the bicopter, and ϕ, θ, and ψ are the roll, pitch, and yaw angles, respectively. The aerodynamic drag force is modeled as:

$$[\mathbf{f}_{\mathrm{d}}]^{\mathrm{B}} = -\frac{1}{2}\rho \mathrm{S}\mathrm{C}_{\mathrm{D}}\|\mathbf{v}_{\mathrm{B}}^{\mathrm{I}}\|[u_{\mathrm{a}}, v_{\mathrm{a}}, w_{\mathrm{a}}]^{\top} \tag{3}$$

where ρ is the air density, S is the reference area, C_{D} is the drag coefficient, and $[u_{\mathrm{a}}, v_{\mathrm{a}}, w_{\mathrm{a}}]^{T}$ are the components of the bicopter's velocity with respect to air. The thrust force generated by the rotors is given by:

$$[\mathbf{f}_{\mathrm{t}}]^{\mathrm{B}} = \begin{bmatrix} \mathrm{b}\Omega_1^2\sin\delta_1 + \mathrm{b}\Omega_2^2\sin\delta_2 \\ 0 \\ -\mathrm{b}\Omega_1^2\cos\delta_1 - \mathrm{b}\Omega_2^2\cos\delta_2 \end{bmatrix} \tag{4}$$

where b is the thrust factor, Ω_i is the angular velocity of the i-th rotor, and δ_i is the tilt angle of the i-th rotor. The moments acting on the bicopter in the body frame are expressed as:

$$[\mathbf{m}]^{\mathrm{B}} = [\mathbf{m}_{\mathrm{d}}]^{\mathrm{B}} + [\mathbf{m}_{\mathrm{t}}]^{\mathrm{B}} \tag{5}$$

where the aerodynamic drag moment is modeled as:

$$[\mathbf{m}_{\mathrm{d}}]^{\mathrm{B}} = \begin{bmatrix} \mathrm{d}(-\Omega_1^2\sin\delta_1 + \Omega_2^2\sin\delta_2) \\ 0 \\ \mathrm{d}(\Omega_1^2\cos\delta_1 - \Omega_2^2\cos\delta_2) \end{bmatrix} \tag{6}$$

where d is the drag factor. The thrust moment generated by the rotors is given by:

$$[\mathbf{m}_{\mathrm{t}}]^{\mathrm{B}} = \begin{bmatrix} \mathrm{ab}(\Omega_1^2\cos\delta_1 - \Omega_2^2\cos\delta_2) \\ -\mathrm{bh}(\Omega_1^2\sin\delta_1 + \Omega_2^2\sin\delta_2) \\ \mathrm{ab}(\Omega_1^2\sin\delta_1 - \Omega_2^2\sin\delta_2) \end{bmatrix} \tag{7}$$

where a is the distance from the CoM to each rotor along the x-axis, and h is the distance from the CoM to each rotor along the z-axis.

C. Equations of Motion

The six degree of freedom dynamic model of the bicopter, based on the Newton–Euler equations and under the flat earth assumption, is derived as follows [14]:

$$\left[\frac{\mathrm{d}\boldsymbol{\omega}^{\mathrm{BI}}}{\mathrm{d}t}\right]^{\mathrm{B}} = \left([\mathbf{I}_{\mathrm{B}}]^{\mathrm{B}}\right)^{-1}\left([\mathbf{m}_{\mathrm{B}}]^{\mathrm{B}} - \left[\boldsymbol{\omega}^{\mathrm{BI}}\right]^{\mathrm{B}} \times [\mathbf{I}_{\mathrm{B}}]^{\mathrm{B}}\left[\boldsymbol{\omega}^{\mathrm{BI}}\right]^{\mathrm{B}}\right) \tag{8}$$

$$\begin{bmatrix} \dot{\phi} \\ \dot{\theta} \\ \dot{\psi} \end{bmatrix} = \begin{bmatrix} 1 & \sin\phi\tan\theta & \cos\phi\tan\theta \\ 0 & \cos\phi & -\sin\phi \\ 0 & \sin\phi\sec\theta & \cos\phi\sec\theta \end{bmatrix} \begin{bmatrix} p \\ q \\ r \end{bmatrix} \tag{9}$$

$$\left[\frac{\mathrm{d}\mathbf{v}_{\mathrm{B}}^{\mathrm{I}}}{\mathrm{d}t}\right]^{\mathrm{B}} = \frac{1}{\mathrm{m}}\left[\mathbf{f}\right]^{\mathrm{B}} - \left[\boldsymbol{\omega}^{\mathrm{BI}}\right]^{\mathrm{B}} \times \left[\mathbf{v}_{\mathrm{B}}^{\mathrm{I}}\right]^{\mathrm{B}} \tag{10}$$

$$\left[\frac{\mathrm{d}\mathbf{s}_{\mathrm{BI}}}{\mathrm{d}t}\right]^{\mathrm{I}} = \mathbf{C}_{\mathrm{B}}^{\mathrm{I}}\left[\mathbf{v}_{\mathrm{B}}\right]^{\mathrm{B}} \tag{11}$$

$\boldsymbol{\omega}^{\mathrm{BI}} = [p, q, r]^T$ is the angular velocity of the bicopter with respect to inertial frame, expressed in body frame, $\mathbf{v}_{\mathrm{B}}^{\mathrm{I}} = [u, v, w]^T$ is the linear velocity of the bicopter in the body frame with respect to inertial frame, expressed in body coordinate, $\mathbf{s}_{\mathrm{BI}} = [x, y, z]^T$ is the position of the bicopter with respect to inertial frame, expressed in the inertial coordinate, $[\mathbf{I}_{\mathrm{B}}]^{\mathrm{B}}$ is the inertia matrix of the bicopter expressed in the body coordinate about the CoM, and $\mathbf{C}_{\mathrm{B}}^{\mathrm{I}}$ is the rotation matrix from the body frame to the inertial frame.

III. Controller Design

In this section, the design of the LQR [14] controller for the bicopter is presented. The LQR controller is chosen for its ability to provide optimal control performance while minimizing a quadratic cost function.

A. Control Command

The input for the bicopter control system consist of the angular velocities of the two rotors, Ω_1 and Ω_2, and the tilt angles of the rotors, δ_1 and δ_2. It is necessary to convert these inputs into total thrust, u_z, and control moments, u_ϕ, u_θ, and u_ψ, to establish a relation between the altitude-channel dynamcis and control commands. The relationship between the rotor inputs and the control commands is given by:

$$u_z = \Omega_1^2\cos\delta_1 + \Omega_2^2\cos\delta_2 \tag{12}$$

$$u_\phi = \Omega_1^2\cos\delta_1 - \Omega_2^2\cos\delta_2 \tag{13}$$

$$u_\theta = \Omega_1^2\sin\delta_1 + \Omega_2^2\sin\delta_2 \tag{14}$$

$$u_\psi = \Omega_1^2\sin\delta_1 - \Omega_2^2\sin\delta_2 \tag{15}$$

B. Control Law

The LQR controller is designed based on the linearized state-space representation of the bicopter dynamics around a hover condition, by minimizing the cost function bellow:

$$\text{cost} = \int_0^t \left(\mathbf{x}^T\mathbf{Q}\mathbf{x} + \mathbf{u}^T\mathbf{R}\mathbf{u}\right)\mathrm{d}t \tag{16}$$

where $\mathbf{x}$ is the state vector, $\mathbf{u}$ is the control input vector, and $\mathbf{Q}$ and $\mathbf{R}$ are weighting matrices that penalize deviations in states and control efforts, respectively. The optimal control law is derived as:

$$\mathbf{u} = -\mathbf{K}\mathbf{x} \tag{17}$$

where $\mathbf{K}$ is the gain matrix obtained by solving the Algebraic Riccati Equation.

IV. Problem Statement

Safe altitude regulation is a fundamental requirement in the operation of bicopters, as deviations in the vertical channel may lead to hazardous situations such as ground impact or violation of altitude restrictions. The altitude-channel dynamics are therefore of particular importance in guaranteeing safe and reliable flight. Traditional controllers are often designed to achieve stabilization and tracking; however, they are susceptible to overshoot, which can drive the vehicle outside its allowable altitude range. Furthermore, the desired altitude commands generated either by the user or by a higher-level path planning algorithm may themselves be unsafe or inconsistent with the system's operational constraints.

To mitigate these risks, the design of a CBF for the altitude-channel is considered. The CBF framework ensures that a predefined safe set for the altitude is forward invariant, even in the presence of inappropriate reference inputs. The key challenge is to construct a barrier function that not only addresses the nonlinear dynamics of the bicopter but also enforces safety against controller overshoot and potentially unsafe altitude references.

The problem can therefore be stated as follows: given the altitude-channel dynamics of a bicopter, the objective is to develop a CBF-based controller that guarantees adherence to altitude safety constraints under all circumstances, including overshoot phenomena and erroneous or unsafe reference inputs, while still enabling the vehicle to accomplish its control objectives.

V. Mathematical Preliminaries

In this section, the fundamental notions of CBFs are concisely presented.

Definition 1 (Class $\mathcal{K}$ function [13])**.** *A mapping $\alpha : [0, a) \to [0, \infty)$, with $a > 0$, is classified as a class $\mathcal{K}$ function if it is continuous, strictly increasing, and satisfies the condition $\alpha(0) = 0$.*

Lemma 1 (Comparison lemma [15])**.** *Consider a function $b : [t_0, t_f] \to \mathbb{R}$ that is continuously differentiable. If:*

$$\dot{b}(t) \geq -\alpha(b(t)), \quad \forall t \in [t_0, t_f]$$

for some class $\mathcal{K}$ function α, and if the initial condition satisfies $b(t_0) \geq 0$, then it follows that $b(t) \geq 0$ for all $t \in [t_0, t_f]$.

Nonlinear affine control systems are considered in the form

$$\dot{\mathbf{x}} = f(\mathbf{x}) + g(\mathbf{x})\mathbf{u} \tag{18}$$

where $\mathbf{x} \in \mathbb{R}^n$, $\mathbf{u} \in \mathbb{R}^m$, and the functions f and g are assumed to be locally Lipschitz.

Definition 2 (Forward invariance)**.** *A set $C \subset \mathbb{R}^n$ is said to be forward invariant for system* (18) *if, for every initial state $\mathbf{x}(t_0) \in C$, the corresponding solution $\mathbf{x}(t)$ remains in C for all $t \geq t_0$.*

Let $b : \mathbb{R}^n \to \mathbb{R}$ be a continuously differentiable function, and define the safe set as:

$$\mathcal{C} = \{\mathbf{x} \in \mathbb{R}^n : b(\mathbf{x}) \geq 0\} \tag{19}$$

Definition 3 (Control Barrier Function (CBF) [11])**.** *The function b is regarded as a candidate CBF for the system* (18) *if there exists a class $\mathcal{K}$ function α such that:*

$$\sup_{u \in U} \left[L_f b(x) + L_g b(x) u + \alpha(b(x)) \right] \geq 0, \quad \forall x \in \mathcal{C} \tag{20}$$

where $L_f b$ and $L_g b$ represent the Lie derivatives of b along the vector fields f and g, respectively.

Theorem 1 (Forward invariance with CBFs [11])**.** *If b qualifies as a CBF associated with the set $\mathcal{C}$ defined in* (19)*, then any Lipschitz continuous control input $\mathbf{u}(t)$ that satisfies* (20) *ensures that $\mathcal{C}$ is forward invariant.*

Definition 4 (Relative degree [16])**.** *The relative degree of a function $b : \mathbb{R}^n \to \mathbb{R}$ with respect to system* (18) *is defined as the minimum number of successive differentiations of b along the system trajectories required before the control input $\mathbf{u}$ explicitly appears.*

In cases where the barrier function b possesses a relative degree greater than one, high-order control barrier functions (HOCBFs) are employed to ensure forward invariance. Let $\psi_i(x)$ represent a set of recursively defined functions obtained from the successive derivatives of $b(x)$.

Definition 5 (High Order CBF (HOCBF) [13])**.** *A function $b : \mathbb{R}^n \to \mathbb{R}$ is called a HOCBF of relative degree m for system* (18) *if there exist differentiable class $\mathcal{K}$ functions α_i, $i = 1, \ldots, m$, such that:*

$$\sup_{u \in U} \left[L_f^m b(x) + L_g L_f^{m-1} b(x) u + O(b(x)) + \alpha_m(\psi_{m-1}(x)) \right] \geq 0 \tag{21}$$

for all x within the safe set. Here, $O(b(x))$ denotes the collection of lower order terms that emerge from the chain rule expansion.

VI. Safety-Critical Control Design

A. Safety Set

In order to guarantees safety, a safety set is defined to represent the safe regions:

$$\mathcal{C} = \{z \subset \mathbb{R} \mid h(z) \geq 0\} \tag{22}$$

$h(z)$ is the barrier function candidate defined as:

$$h(z) = (z - z_{\min})^2 - \mathrm{D}^2 \tag{23}$$

where z denotes the altitude of the bicopter, and $z_{\min}$ represents the lower altitude bound, which corresponds to the negative of the obstacle height, and d is a positive constant that defines the minimum allowable distance from the obstacle.

$$\begin{aligned} \mathcal{U} = \{u = u_z \subset \mathbb{R} \mid \\ L_f^2 h(z) + L_g L_f h(z) u + \beta L_f h(z) + \alpha h(z) \geq 0\} \end{aligned} \tag{24}$$

α and β are positive design parameters that determine the convergence rate to the safe set boundary. To ensure the convergence, the following condition must be satisfied:

$$\beta^2 - 4\alpha \geq 0 \tag{25}$$

B. Formulating QP Problem

In every time step, the following QP is solved to find the optimal safe control input that is as close as possible to the nominal control input u_{LQR} from LQR controller while ensuring safety:

$$\begin{aligned} u^* = \underset{u \in \mathbb{R}}{\operatorname{argmin}} \ & \|u - u_{\mathrm{LQR}}\|^2 \\ \text{s.t.} \quad & \mathrm{a}u \leq \mathrm{b} \end{aligned} \tag{26}$$

where $\mathrm{a} = L_g L_f h(z)$ and $\mathrm{b} = -L_f^2 h(z) - \beta L_f h(z) - \alpha h(z)$.

VII. Simulation Results

To validate the effectiveness of the proposed safety-critical control strategy, simulation was conducted using MATLAB/Simulink. The bicopter is tasked to track a step commands of x = 5 m, y = 4 m, and h = -z = 12 m, starting from the origin with zero initial velocities and orientations. The simulation parameters are listed in Table I. The lower altitude bound is set to $z_{\min} = -10$ m, and the minimum allowable distance from the obstacle is set to $\mathrm{D} = 1$ m. The design parameters for the CBF are chosen as $\alpha = 30$ and $\beta = 11$. Fig. 3 illustrates the height response of the bicopter with and without the CBF-based safety controller. Without the CBF, the bicopter violates the safety constraint by passing through the unsafe region over $\mathrm{h}_{\max} \equiv -\mathrm{z}_{\min}$. In contrast, with the CBF in place, the bicopter successfully maintains its height within the safe set, demonstrating the effectiveness of the safety-critical control strategy. Fig. 4 shows the bicopter's translational motion in the x and y directions, indicating that the safety controller does not adversely affect the lateral dynamics. The bicopter is able to reach the desired x and y positions while adhering to the altitude channel safety constraints.

TABLE I: Simulation Parameters

Parameter	Value
Mass, m (kg)	0.296
Gravity, g (m/s^2)	9.81
Air density, ρ (kg/m^3)	1.2682
Reference area, S (m^2)	0.25
Drag coefficient, C_D	0.32
Parameter b	2.98×10^{-6}
Parameter a	0.225
Parameter h	0.0225
Parameter d	1.14×10^{-7}

Fig. 5 illustrates the control inputs generated by both the LQR controller and the CBF. CBF modifies the control inputs to ensure that the altitude remains within the predefined safe set, particularly during instances where the LQR controller's

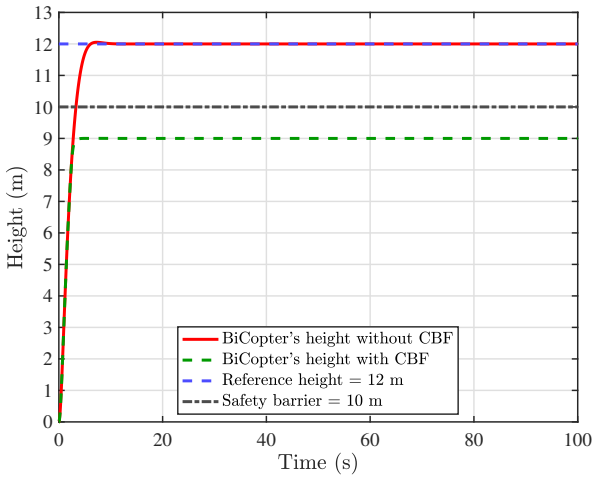

Fig. 3: Bicopter's height position over time with and without CBF

commands would have led to unsafe conditions. By converting the control inputs to rotor speeds and tilt angles using 27, 28, 29, and 30, as shown in Fig. 6, Fig. 7, Fig. 8, and Fig. 9, the safety-critical controller effectively adjusts these parameters to maintain safety without significantly deviating from the nominal control strategy.

$$\delta_1 = \arctan\left(\frac{u_\theta + u_\psi}{u_z + u_\phi}\right) \tag{27}$$

$$\delta_2 = \arctan\left(\frac{u_\theta - u_\psi}{u_z - u_\phi}\right) \tag{28}$$

$$\Omega_1 = \sqrt{\frac{(u_z + u_\phi)}{\mathrm{b}\cos\delta_1}} \tag{29}$$

$$\Omega_2 = \sqrt{\frac{(u_z - u_\phi)}{\mathrm{b}\cos\delta_2}} \tag{30}$$

VIII. Conclusion

As a conclusion, this paper presents a safety-critical control strategy for a tilt-rotor bicopter using Control Barrier Functions (CBFs). The proposed method effectively ensures that the bicopter maintains safe height levels while following desired trajectories. It is also shown that the designed CBF does not adversely affect the translational motion of the bicopter in x and y directions. Simulation results validate the effectiveness of the approach, demonstrating that the bicopter can successfully avoid unsafe altitude regions while adhering to control objectives. Future work may involve combining the CBF with other advanced control techniques to enhance overall system robustness in landing scenarios. For instance, integrating the CBF with an observer could help estimate unmeasured states or disturbances, further improving safety and performance.

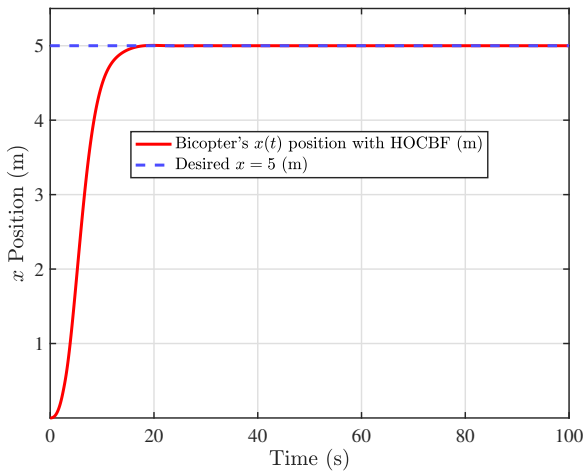

(a) x position over time

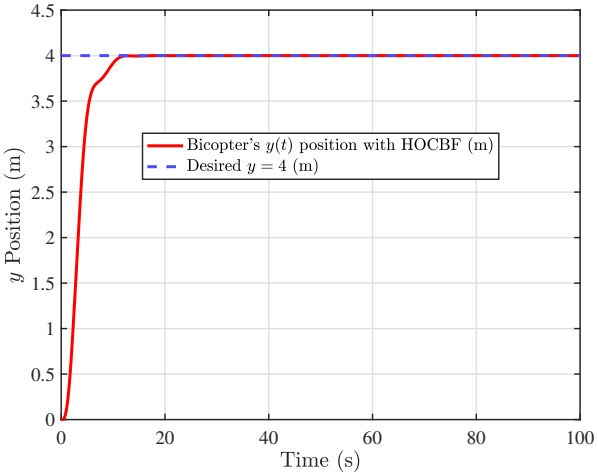

(b) y position over time

Fig. 4: Bicopter's translational motion: (a) x position and (b) y position with respect to time.

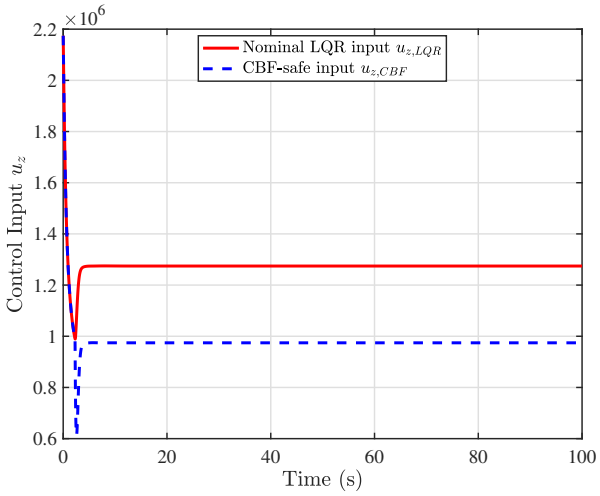

Fig. 5: Control inputs from LQR and CBF

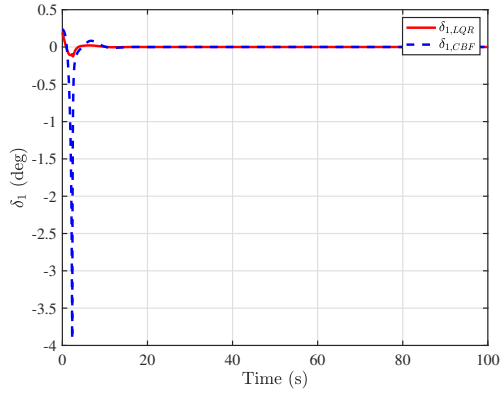

Fig. 6: Tilt angle of motor 1 (deg) over time

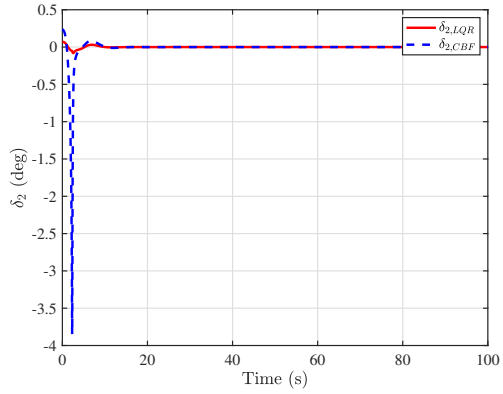

Fig. 7: Tilt angle of motor 2 (deg) over time

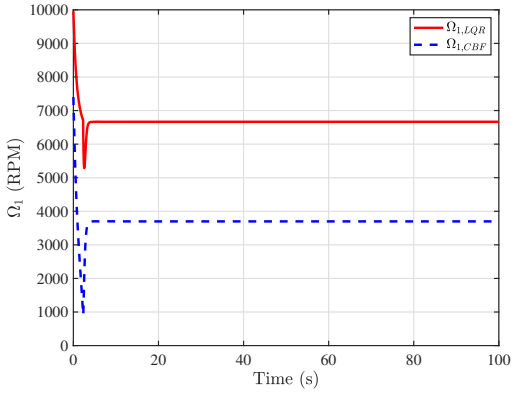

Fig. 8: Angular speed of motor 1 (RPM) over time

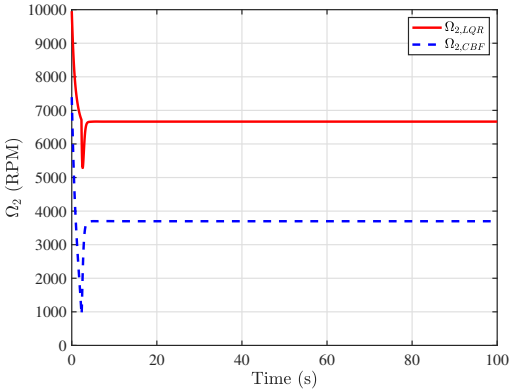

Fig. 9: Angular speed of motor 2 (RPM) over time

REFERENCES

[1] F. Gonçalves, J. Bodanese, R. Donadel, G. Raffo, J. Normey-Rico, and L. Becker, "Small scale uav with birotor configuration," in *2013 International Conference on Unmanned Aircraft Systems (ICUAS)*. IEEE, 2013, pp. 761–768.

[2] C. Papachristos, K. Alexis, and A. Tzes, "Design and experimental attitude control of an unmanned tilt-rotor aerial vehicle," in *2011 15th International Conference on Advanced Robotics (ICAR)*. IEEE, 2011, pp. 465–470.

[3] L. Hrečko, J. Slačka, and M. Halás, "Bicopter stabilization based on imu sensors," in *2015 20th International Conference on Process Control (PC)*. IEEE, 2015, pp. 192–197.

[4] C. Blouin and E. Lanteigne, "Pitch control of an oblique active tilting bi-rotor," in *2014 International Conference on Unmanned Aircraft Systems (ICUAS)*. IEEE, 2014, pp. 791–799.

[5] Q. Zhang, Z. Liu, J. Zhao, and S. Zhang, "Modeling and attitude control of bi-copter," in *2016 IEEE International Conference on Aircraft Utility Systems (AUS)*. IEEE, 2016, pp. 172–176.

[6] Ö. B. Albayrak, Y. Ersan, A. S. Bağbaşı, A. T. Başaranoğlu, and K. B. Arıkan, "Design of a robotic bicopter," in *2019 7th International Conference on Control, Mechatronics and Automation (ICCMA)*. IEEE, 2019, pp. 98–103.

[7] Y. Li, Y. Qin, W. Xu, and F. Zhang, "Modeling, identification, and control of non-minimum phase dynamics of bi-copter uavs," in *2020 IEEE/ASME International Conference on Advanced Intelligent Mechatronics (AIM)*. IEEE, 2020, pp. 1249–1255.

[8] C. Papachristos, K. Alexis, G. Nikolakopoulos, and A. Tzes, "Model predictive attitude control of an unmanned tilt-rotor aircraft," in *2011 IEEE International Symposium on Industrial Electronics*. IEEE, 2011, pp. 922–927.

[9] A. Abedini, A. A. Bataleblu, and J. Roshanian, "Robust backstepping control of position and attitude for a bi-copter drone," in *2021 9th RSI International Conference on Robotics and Mechatronics (ICRoM)*. IEEE, 2021, pp. 425–432.

[10] H. A. Nugroho, A. I. Cahyadi, I. Ardiyanto *et al.*, "Trajectory tracking control of uav bicopter using linear quadratic gaussian," *arXiv preprint arXiv:2309.08226*, 2023.

[11] A. D. Ames, S. Coogan, M. Egerstedt, G. Notomista, K. Sreenath, and P. Tabuada, "Control barrier functions: Theory and applications," in *2019 18th European control conference (ECC)*. Ieee, 2019, pp. 3420–3431.

[12] Y. Wang, "Trajectory tracking control of quadrotors via robust control barrier function," in *2024 43rd Chinese Control Conference (CCC)*. IEEE, 2024, pp. 2239–2244.

[13] W. Xiao and C. Belta, "High-order control barrier functions," *IEEE Transactions on Automatic Control*, vol. 67, no. 7, pp. 3655–3662, 2022.

[14] B. D. Anderson and J. B. Moore, *Optimal control: linear quadratic methods*. Courier Corporation, 2007.

[15] H. K. Khalil and J. W. Grizzle, *Nonlinear systems*. Prentice hall Upper Saddle River, NJ, 2002, vol. 3.

[16] W. Xiao and C. Belta, "Control barrier functions for systems with high relative degree," in *2019 IEEE 58th conference on decision and control (CDC)*. IEEE, 2019, pp. 474–479.